Analytical load rating of an open spandrel arch bridge: case study

G.P. Garrett
URS Corporation, Grand Rapids, Michigan, United States

ABSTRACT: The live load structural capacity of open-spandrel arch bridge structures is difficult to quantify. In addition to live and dead loads, geometric nonlinear effects, temperature effects, and material behavior play key roles in the design and load rating of such a structure. This paper is a case study that illustrates the effect these variables have on load rating a two-span shallow concrete arch bridge. Presented are load ratings of the structure's arch ribs using a three-dimensional finite-element model with American Association of State Highway and Transportation Officials publications. As a result of this study, a refined analysis is recommended for load rating arch bridges.

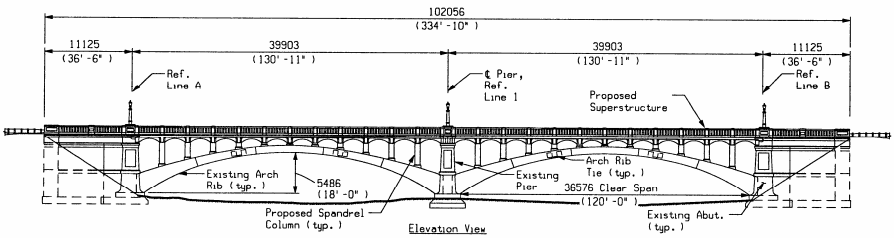

Figure 1: Elevation view of the Paint River bridge.

1. INTRODUCTION

The main objective of this paper is to present an example of load rating an arch bridge using the Manual for Condition Evaluation of Bridges (MCE) (AASHTO 1994) as a guide in conjunction with the American Association of State Highway and Transportation Officials Standard Specifications for Highway Bridges (Standard Specifications) (AASHTO 2002). It represents the author's interpretation of the documents in performing a load rating of a concrete open spandrel arch bridge. The MCE gives little guidance to load rate this type of structure and the analysis procedures of the Standard Specifications were assumed by the author to be conservative. To date, not much has been published on load rating concrete arch bridges and the author was compelled to investigate various methods of analysis in an effort to better quantify the structures rating. The load rating of a structure is an estimate of its live load carrying capacity.

The second objective is to illustrate nonlinear effects on the analysis and subsequent load rating of an arch bridge. The effects of in-plane deformations on an arch bridge has already been discussed by Asplund (1963), and Austin et al. (1982). In this paper, a brief explanation of nonlinear analysis is given with detailed steps of a simplified method, as described by Nawy

(1995) and O'Connor (1971), used to evaluate this structure. The results of the investigation are shown and compared with a base-line elastic analysis and the Standard Specifications method of Moment Magnification.

Crystal Falls is a small town located in Michigan's upper-peninsula. Just east of town is a historic two span open spandrel arch bridge, built in 1929, that carries route M69 over the Paint River. The bridge span lengths and geometry are shown in Figure 1. It carries two lanes and sidewalks across the Paint River with cross section dimensions as shown in Figure 2 (a).

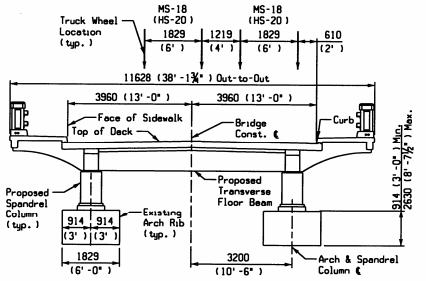

(a)

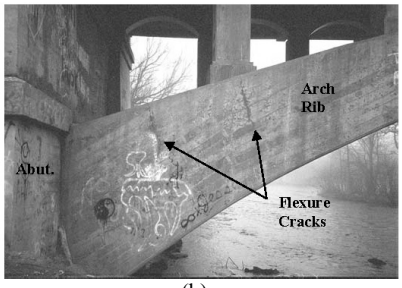

(b)

Figure 2: (a) Typical bridge section showing truck placement; (b) Photograph of typical existing cracks in the arch ribs.

The main structural elements of the bridge are two concrete arch ribs supporting each span with the dimensions shown in Figure 2 (a). The shallow arch has a clear rise to span ratio of about 0.15 and fixed-fixed support conditions. The bridge has been recently rehabilitated, which involved reconstructing everything above the arch ribs for both spans. The new concrete deck is fixed at the pier location and is continuous along the entire length of the bridge. The forces generated from expansion and contraction of the jointless deck outwards from the pier are released by expansion joints at the approaches. Elastomeric bearings provided at the top of each spandrel column are guided and allow the superstructure to move in the longitudinal direction, but restrain transverse movements

A typical beam-slab bridge structure is composed of a concrete deck slab over longitudinal beams where the use of a general elastic analysis is sufficient, as specified by the MCE, for performing a load rating. An open spandrel arch bridge is different because the arch ribs are primarily compression members, where deformations and slenderness play a vital role in the analysis of an arch. Secondary forces result from deflections of the arches and should be accounted for in the analysis, design, and/or load rating. The MCE is mainly intended for the evaluation of common bridge structures, not for more complex structures such as arch, suspension, cable-stayed, etc. However, it may be used as a guide for evaluating such structures.

2. RATING

The rating of a bridge can be performed using the basic AASHTO rating equations given in the MCE. The equations, applied to the various components that make up a bridge, can determine the controlling component of a bridge and the components rating. This discussion is limited to rating only the arch ribs because the bridge recently received a new superstructure, and spandrel columns. The criteria for determining the capacity of the arch ribs was based on the standard code provisions for strength design resulting from strain compatibility. The Load Factor Design method was used for all analysis.

The loading used for rating includes dead load and live load for the Inventory rating, and typically dead load, live load, sidewalk live load, and environmental loads (temperature, wind, etc.) for the Operating rating. The dead load applied to the arches other than their own weight, include the spandrel columns, transverse beams, roadway deck, sidewalk, and barrier. Two

MS-18 (HS-20) trucks were used for live load, one in each lane for this study. The sidewalk live load was included in the Operating Rating as per the MCE. The rating of arch bridges differs from the typical short to medium span bridge in that thermal effects should be considered as per the MCE for the Operating rating. Thermal loading was applied to the arches for a "Cold climate" temperature rise of 19°C (35°F) and temperature fall of –25°C (-45°F). The temperature changes were assumed to act uniformly along the entire arch. A temperature gradient along the depth of the arches, similar to what is specified in the AASHTO Guide Specifications Thermal Effects in Concrete Bridge Superstructures (1989), was not applied due to the uncertainty of how, where, and to what extent the gradients would occur along the arch ribs.

The ratings of the arches included Inventory and Operating with and without temperature, for a first order analysis, second-order analysis using moment magnification, as well as a second-order analysis using a refined P-delta method. All of the arch ribs have cracks at about the same location along their length as shown in Figure 2 (b). These cracks, representative of flexural cracking, are evidence the stresses in the arch ribs have at some point exceeded the modulus of rupture for concrete. As a result, redistribution of elastic forces, i.e. moments, occurs in the arch ribs, affecting the ratings. The author believes it is important to illustrate the significance of this effect on the first-order, as well as the second-order ratings. The ratings resulting from moment redistribution were included as an upper-bound. Two results were found for each rating, one neglecting moment redistribution due to the cracks, and the other considering moment redistribution as a result of the cracked regions.

3. FINITE ELEMENT MODEL

The two-span structure was modeled with the software STAAD.PRO 2002. Figure 3 (a) is a view of the entire bridge model as it was represented in STAAD with 268 elements and 192 nodes. Beam type elements were used throughout with six degrees of freedom at each node. Each individual arch rib was modeled as a composition of 24 beam elements, each with different cross-sectional properties representing the arch depth variation from spring point to crown. The arch ribs could have been modeled with a larger number of elements, but as shown by W. Austin et al. (1982), as few as 24 elements may be adequate for two-hinged parabolic and fixed circular arches. To verify the arch rib model, a three-dimensional arch rib model containing 864 solid, eight-noded isoparametric type finite elements was created and compared to the 24 beam element arch rib model with dead load and a simplified live load case. The higher degree of freedom model, with an improved representation of the varying arch rib geometry, was used to investigate whether the deflections and stresses in the arches were sensitive to mesh size, element type, and model geometry and how sensitive. The largest variation of output between models for elastic in-plane deflections was found to be less than 5%. The 24 beam element model produced average stress results that were 18% higher than the large element model. However, because direct shrinkage and creep effects were neglected, the conservative results of the simple model were considered acceptable by the author. A hand-verification was also performed on the 24 beam element arch rib using the Elastic Center method as shown by Dunham (1939). Influence lines were generated for reaction forces at the abutment and were in agreement with the 24 beam element STAAD model. Therefore, the 24 beam element model was used for all analysis.

The spandrel columns and superstructure were modeled to represent the new member cross-sectional and material properties. The existing plans contained limited material information and material sampling could not be performed. So, the existing concrete compression strength was assumed as f'c = 17.2 MPa (2500 psi) for the arch ribs, pier, and rib ties. The steel reinforcement yield strength was assumed as fy = 227.5 MPa (33 ksi). These values are representative of bridges constructed around 1930 according to the MCE.

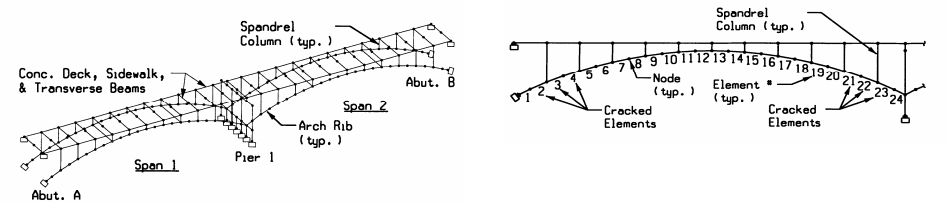

(a) (b)

Figure 3: (a)Three-dimensional view of bridge finite-element model; (b) Partial screen capture of arch rib three

The arch ribs were visually inspected for section loss and cracking with only a few areas of cracking found. Two models were created, one without incorporating cracking, and the other with cracked elements, as shown in Figure 3 (b), having a reduced moment of inertia (I). The cracks present in the arch ribs were tightly closed without the presence of efflorescence or rust. So, reinforcement losses were assumed to be negligible. This assumption was confirmed during the rehabilitation construction when the existing reinforcement was exposed and found in excellent condition. The arch ribs were cracked at approximately the same location in both spans, see Figure 3 (b). Field measurements of crack locations, length, and width were taken at several times throughout the year. The cracks had a length of 40% of the arch depth. The cracked model incorporated an effective moment of inertia (I_e) for elements correlating to cracked sections based on the Standard Specifications. The average resulting effective inertia (I_e) for these members was 51% of the gross inertia (I_g).

The vehicle live load applied to the model for rating consisted of two MS-18 (HS-20) trucks, side by side in the configuration shown in Figure 2 (a). Crowding the trucks into 3 m (10 ft) lanes was a reflection of observed conditions on the bridge in which vehicles crowd, and in some instances cross the bridge centerline due to a horizontal curve adjacent the structure. The truck positioning produced the maximum effect on a single arch rib resulting in an arch rib distribution factor of 1.25 lanes. The trucks were moved together along one span of the bridge model in 1.520 m (5 ft) increments. Sidewalk live load was applied to the spandrel columns based on tributary area of the sidewalk above each column. Thermal fall, the controlling temperature load, was performed on the model by applying a uniform temperature change to the entire model.

A first-order and second-order refined analysis and rating was performed with the use of STAAD. STAAD will perform a second-order analysis for frame-members using the initial elastic deflections. However, because long-term deflections or material deflection effects contribute much to a geometric nonlinear analysis, the second-order effects would have to be incorporated. Long-term deflections could be accounted for by reducing the modulus of elasticity by the long-term deflection coefficient, but the author determined that this was invalid because the force generated by temperature loading, which is a strain load, is directly proportional to the modulus of elasticity. The temperature forces would drop dramatically and would not have been comparable to the other models. Therefore, the second-order effects would have to be calculated and incorporated into the first-order model.

4. ELASTIC ANALYSIS AND MOMENT MAGNIFICATION

The elastic analysis output from STAAD was used for the first order (elastic) ratings as well as the ratings with moment magnification, which is a single-step approximation of geometric second-order effects (AASHTO 2002). The STAAD model results for biaxial moment from load forces acting on each arch rib element were applied to a model of each element in the software PCACOL. PCACOL was then used to create the axial-moment (P-M) failure surface and compute the ratio of applied forces to design strength of each element section based on a biaxial, ultimate strength analysis. The critical element was the second arch element from the

abutment, or pier, labeled 2 and 23 in Figure 3 (b). These element locations correlated well with the crack locations of each rib as shown in Figure 2 (b).

Once the critical element was located, rating of the arch ribs could be performed with the ratios resulting from PCACOL, in conjunction with the MCE rating equations. The first-order ratings were found for the uncracked and cracked model and are shown in Table 1.

The AASHTO code provisions for a second-order analysis include an approximate, one step method using moment magnification, which accounts for slenderness effects in the vertical plane of the arch. The slenderness ratio of the concrete arch rib was calculated following the AASHTO code provisions and was approximated as 41.1. This slenderness value required the use of a magnified moment, Mc, determined using equations of the Standard Specifications. The moment magnifier, δ_b, for members braced against sidesway, was found following the Standard Specifications for Inventory and Operating rating and used to calculate the magnified moments, Mc. The magnified moments were then input into PCACOL and the ratings calculated similar to the elastic first-order analysis and are shown in Table 1. The Inventory, Operating, and Operating rating less temperature were also found using the model with force redistribution effects resulting from cracked arch rib members as shown in Table 1.

Table 1. Load rating results

Method/model	Inventory rating (without temperature fall)		Operating rating (with temperature fall*)		Operating rating (without temperature fall)	
	MS (HS)	tonne (tons)	MS (HS)	tonne (tons)	MS (HS)	tonne (tons)
First-order elastic/uncracked	44 (49)	81(89)	17 (19)	31(34)	71 (79)	130(143)
First-order elastic/cracked	59 (66)	107(118)	51 (57)	93(102)	95 (106)	173(191)
Second-order moment magnification/uncracked	30 (33)	54(60)	4 (5)	8(9)	59 (66)	108(119)
Second-order moment magnification/cracked	41 (46)	74(82)	35 (39)	64(71)	80 (89)	146(161)
Second-order P-delta/uncracked	42 (47)	76(84)	9 (10)	16(18)	67 (75)	122(135)
Second-order P-delta/cracked	54 (61)	99(109)	43 (48)	78(86)	91 (101)	165(182)

*Temperature drop of -25 degrees Celsius (-45 degrees Fahrenheit).

5. SECOND-ORDER ANALYSIS PROCEDURE

Second-order effects consist of nonlinear geometric effects and nonlinear material effects. Nonlinear geometric effects can be divided into those resulting from sidesway deflections (Δ) of a member under compression as shown in Figure 4 (a), and change in curvature, or deflection (δ) along the span of a member under compression (Figure 4 (b)). The rating performed on this structure included only global geometric effects resulting from deflection (δ), along the arch ribs represented by deflection of the straight rib elements, or rigid body deflections as will be shown. Change in curvature of the individual elements that make up each arch rib was not evaluated, and contributions due to shear deformations were also not included.

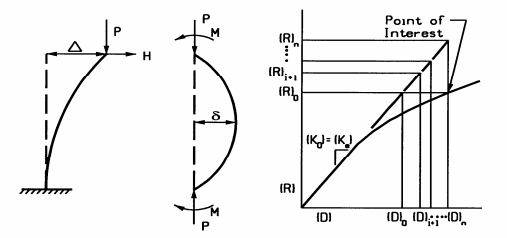

Figure 4: (a) Compression member subject to sidesway deflections; (b) compression member subject to change in curvature; and (c) graphic representation of second-order analysis.

Material nonlinear effects consist of concrete time-dependent effects such as creep and shrinkage, and time-independent effects that include cracking and the nonlinear stress-strain relationship of concrete. They can cause the forces in a structure to redistribute and influence nonlinear geometric effects resulting from deflections. The material nonlinear influence on deflections was estimated per the Standard Specifications. A long term deflection coefficient of four was used because the model incorporated the gross moment of inertia (I_g) for all arch rib elements of the uncracked model and all arch rib elements of the cracked model except the visibly cracked areas close to the spring points. This value was applied to elastic dead load and temperature deflections, which were then used for the second-order analysis.

Various methods are available to perform a second-order structural analysis including Direct Substitution, Newton-Raphson or Load Control Method, Modified Newton-Raphson, Incremental Methods, Arc Length Method, the Displacement Control Method, etc. as described by Cook (1989) et. al. Commercial software available today will typically employ one of the aforementioned methods to evaluate the geometric nonlinear effects on a structure.

The commercial software available to the author, STAAD-Pro 2002, for evaluating the Paint River structure will perform a second-order analysis, or a geometric nonlinear analysis similar to the Newton-Raphson method for a frame model. However, this version of software uses initial elastic deflections, and long-term deflections are important to a geometric nonlinear analysis. Therefore, the author needed to use a method in conjunction with the first-order STAAD model analysis that would produce acceptable geometric nonlinear effects. The method also needed to be practical enough so that it could be applied to the four arches of the bridge during multiple iterations without being too analytically cumbersome.

The method used by the author is similar to a second-order analysis for a building structure as described by Nawy, et. al. It involves four steps and is shown graphically in Figure 4 (c). A first-order analysis was initially performed using the previously described model in STAAD. Structural deformations result from this analysis as given by the usual first-order stiffness matrix formulation:

$$\mathbf{[D]}_0 = \mathbf{[K_e]}^{-1}\mathbf{[R]}_0 \tag{1}$$

Where $\mathbf{[D]}_0$ are initial elastic deformations of a structure, $\mathbf{[K_e]}^{-1}$ is the inverse of the structure elastic stiffness matrix, and $\mathbf{[R]}_0$ is the initial structure load vector. The second step involves using $\mathbf{[D]}_0$ along with axial loads to produce second-order correction loads. The correction loads are then applied to the STAAD model for the third step and another analysis is performed with the updated load vector $\mathbf{[R]}_1$ producing a new deformation vector $\mathbf{[D]}_1$. Step four involves a convergence check of the new deformations based on criteria set by the author as 0.5% difference between iterations. If the convergence-criteria is not met, the third and fourth steps are repeated until convergence is achieved. Once the convergence-criteria is met, the resulting structural deformations $\mathbf{[D]}_i$ and element forces resulting from $\mathbf{[R]}_i$ may be considered the second-order results. The application of this method as applied to the arch ribs of this structure will be explained further to illustrate the inclusion of a deflection coefficient multiplier as per the Standard Specifications and realistic loading conditions.

The calculation of second-order correction loads was performed using a procedure described by Colin O'Connor, et al. Loads approximating second-order effects in the plane of the arch were calculated from dead load, temperature, and vehicle live load deflections and applied to the first order STAAD model. The dead load and temperature effects were found for all elements of each arch rib. However, the live load was placed at the same location as the other analysis procedures to have a maximum effect on element 2 of Figure 3 (b). At the element level a first-order stiffness matrix analysis has the form:

$$\mathbf{[r]} = \mathbf{[k_e][d]} \tag{2}$$

In equation 2, $\mathbf{[k_e]}$ is the element elastic stiffness matrix, **[d]** are the element distortions, and **[r]** are the resulting forces applied to an element. Element joint loads **[P]** can be calculated from the element forces using:

$$\mathbf{[P]} = \mathbf{[A][r]} \tag{3}$$

Where **[A]** is the common static matrix. To approximate second-order effects, a correction system of joint loads may be added to the first-order system. These correction loads are based on axial loads, and displacements of the arch elements. The correction system has the form:

$$\mathbf{[P']} = \mathbf{[C][X]} \tag{4}$$

Which, for a typical element, appears as:

$$\begin{bmatrix} X_3 \\ Y_3 \\ M_{34} \\ X_4 \\ Y_4 \\ M_{43} \end{bmatrix} = \begin{bmatrix} -\frac{Ts^2}{1} & \frac{Tsc}{1} & 0 & \frac{Ts^2}{1} & -\frac{Tsc}{1} & 0 \\ \frac{Tsc}{1} & -\frac{Tc^2}{1} & 0 & -\frac{Tsc}{1} & \frac{Tc^2}{1} & 0 \\ (-Ts) & (Tc) & (0) & 0 & 0 & 0 \\ \frac{Ts^2}{1} & -\frac{Tsc}{1} & 0 & -\frac{Ts^2}{1} & \frac{Tsc}{1} & 0 \\ -\frac{Tsc}{1} & \frac{Tc^2}{1} & 0 & \frac{Tsc}{1} & -\frac{Tc^2}{1} & 0 \\ 0 & 0 & 0 & \{Ts\} & \{-Tc\} & \{0\} \end{bmatrix} \times \begin{bmatrix} u_3 \\ v_3 \\ \theta_3 \\ u_4 \\ v_4 \\ \theta_4 \end{bmatrix} \tag{5}$$

Where "T"= element thrust, "s"= sin α, and "c"= cos α. The angle α, is the initial angle between an element and the horizontal plane before any deflections have taken place. The terms in parentheses ( ) are only included for the element at the left end of the arch and the terms in brackets { } are only included for the element at the right end. The joint deflections and rotation, u_i, v_i, and θ_i are for the coordinate system shown in figure 5 (a). The joint loads, including the additional correction system, can be determined with the following equation:

$$\mathbf{[P]} = \mathbf{[A][F]} + \mathbf{[P']} \tag{6}$$

A spreadsheet was used to calculate the correction loads, **[P']**, of each element, for each arch.

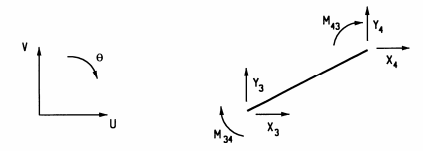

(a) (b)

Figure 5: (a) Coordinate system for joint deflections and rotations; (b) correction loads applied to a typical arch element (Reprinted with permission from John Wiley & Sons, Inc.).

The correction loads were calculated for dead load, temperature, and live load with a long-term deflection multiplier of four applied to dead load and temperature deflections. The dead load correction system was computed using thrust and deflections resulting from dead load. The temperature correction system resulted from dead load and temperature thrust, and temperature deflections. The live load correction loads were computed based on thrust from dead load, temperature, and live load, and live load deflections. The resulting ratings from nonlinear analysis are shown in Table 1.

6. OBSERVATIONS

An investigation was undertaken to determine the Inventory and Operating load rating capacity for an open-spandrel concrete arch structure. The bridge spandrel columns and superstructure have been reconstructed, so the ratings found were based solely on analyzing the arch ribs.

The resulting ratings listed in Table 1 show that, as expected, the elastic analysis resulted in the highest live load ratings. The ratings resulting from the Moment Magnification method were lower than the Elastic analysis as expected. The Inventory rating was approximately 32% less than the Elastic method, averaged 52% less for the Operating rating with a thermal fall loading included, and 16% less for Operating rating neglecting the thermal effects. The difference between these two methods is substantial, especially in the context of this structure, a shallow, short span structure with arch ribs having a relatively low slenderness value.

The Standard Specifications direct the engineer to use a more rigorous analysis for compression members having a slenderness ratio greater than 100. A refined analysis may also be required by some agencies to determine the permit loads allowed on a bridge with greater accuracy. The incremental process for this bridge converged fairly quickly with only three increments. This can be attributed to the small initial elastic deflections in the plane of the arch ribs, relatively low axial loads, and that the contributions from deformations out of the plane of the arches and shear were not included in the analysis. The Inventory rating by the P-delta method averaged 36% more than the Moment Magnification method and about 7% less than the Elastic rating. The Operating rating by the P-delta method, which included temperature fall effects, was an average of about 61% more than the Moment Magnification method and 31% less than the Elastic rating. The Operating rating resulting from the second-order analysis without temperature effects was about 13% more than the Moment Magnification method and about 5% less than the Elastic rating.

It should be noted that the deflection multiplier based on the Standard Specifications was used for both the cracked and uncracked models. Therefore, some overlap resulted for the cracked model because even though the cracked model used a reduced moment of inertia for the visibly cracked elements of the arch ribs, the arch deflections were multiplied by the same multiplier recommended by the Standard Specifications for gross moment of inertia. The cracked model used a reduced inertia (I_e) for only the six visually cracked elements out of 24 for each arch rib. The author felt that this should require a reduced multiplier, but the current Standard Specifications have only two equations, one for the gross inertia (I_g), and one for a reduced effective inertia (I_e). I_e could be used for the entire arch in a further refined analysis for comparison.

The effect of force redistribution due to cracking of the arch ribs is evident by the values of Table 1. The minimum rise in rating was 30% when comparing the cracked verses uncracked model results. Although the cracked model used an effective inertia (I_e) for each entire cracked element and not just the finite crack location in each element, the results may be considered an upper bound.

The refined analysis used for this study was simplistic, but considered to be adequate by the author. A future study could also include a space-frame geometric nonlinear analysis, as discussed by Yang and Kuo, incorporating out of plane deformations of the arch ribs.

The temperature ranges applied to this structure were uniform for the entire model. The load ratings shown in Table 1 illustrate the severe effects temperature ranges can have on a structure of this type. The uniform thermal loads produced ratings at least 47% less than ratings without thermal loads and may be unduly conservative.

The one-step Moment Magnification method included in the Standard Specifications may be quite conservative for a relatively shallow, open spandrel concrete arch bridge similar to the Paint River structure. A refined analysis is recommended by the author to load rate similar structures. Although it requires more effort, a refined analysis is a closer approximation of the rating and may be the difference between rehabilitation and much more costly replacement and the loss of a historic structure.

The author feels the Paint River bridge rating should not be based solely on the results of this study. The observed performance of the arch ribs is also a consideration. Though cracks in the ribs are present, they have existed for some time, are tight, and appear to be stable with no leaching or rust stains visible. The analytical Operating rating of this structure was taken as an

average of the P-delta cracked and un-cracked, with and without temperature, resulting in a rating of MS-53 (HS-59). Finally, nondestructive, or proof-load testing may be used to further rate or confirm the analytical rating of an open spandrel arch bridge, as shown by Lai (1995).

REFERENCES

American Association of State Highway and Transportation Officials (AASHTO). (2002). *Standard Specifications for Highway Bridges*, 17th edition. Washington, D.C.

American Association of State Highway and Transportation Officials (AASHTO). (1994). *Manual for Condition Evaluation of Bridges*, 2nd edition. Washington, D.C.

Asplund, S. O., (1963). "Deflection Theory of Arches" *Transactions*, ASCE, 128(part II), 307-341.

Austin, W. J., Ross T. J., Tawfik A.S., and Volz, R. D., (1982). "Numerical Bending Analysis of Bridges" J. of Str. Div., ASCE, 108(4), 849-868.

Cook, R. D., Malkus, D. S., Plesha, M.E., (1989). *Concepts and Applications of Finite Element Analysis* John Wiley & Sons, Inc., 501-533

Dunham, Clarence, (1939). *Theory and Practice of Reinforced Concrete,* McGraw Hill, 391-409

Lai, L.L.-Y. (1995). "Rating of an open-spandrel concrete arch bridge by load testing." *Proc., Restructuring: America & Beyond*, ASCE, Reston, VA., 1329-1332.

Nawy, Edward G.,(1995). *Prestressed Concrete: A Fundamental Approach* Prentice Hall International, 521-522

O'Connor, Colin, (1971). *Design of Bridge Superstructures* John Wiley & Sons, Inc., 528-532

PCACOL user's manual-version 2.30. (1993). Portland Cement Association.

STAAD Pro Technical Reference-version 2002 (2002). Research Engineers, Intl., a division of netGuru, Inc.

Yang, Y., Kuo, S., (1994). *Theory & Analysis of Nonlinear Framed Structures* Prentice Hall, 146-215, 491-557